12-2002

Evolution of a Monomer Concentration Field in a Micro-Fluidic Channel

Michael Francis Kirsch
University of Tennessee - Knoxville

To the Graduate Council:

I am submitting herewith a thesis written by Michael Francis Kirsch entitled "Evolution of a Monomer Concentration Field in a Micro-Fluidic Channel." I have examined the final electronic copy of this thesis for form and content and recommend that it be accepted in partial fulfillment of the requirements for the degree of Master of Science, with a major in Aerospace Engineering.

Dr. Basil Antar, Major Professor

We have read this thesis and recommend its acceptance:

Dr. Frank Collins, Dr. Kenneth Kimble

Accepted for the Council:
Carolyn R. Hodges

Vice Provost and Dean of the Graduate School

(Original signatures are on file with official student records.)

To the Graduate Council:

I am submitting herewith a thesis written by Michael Francis Kirsch entitled "Evolution of a Monomer Concentration Field in a Micro-Fluidic Channel." I have examined the final electronic copy of this thesis for form and content and recommend that it be accepted in partial fulfillment of the requirements for the degree of Master of Science, with a major in Aerospace Engineering.

_____Dr. Basil Antar_____
Basil N. Antar, Major Professor

We have read this thesis and
Recommend its acceptance:

____Dr. Frank Collins_____

___Dr. Kenneth Kimble____

Accepted for the Council:

__Dr. Anne Mayhew_____
Vice Provost and Dean of
Graduate Studies

(Original signatures are on file with official student records)

EVOLUTION OF A MONOMER CONCENTRATION FIELD IN A MICRO-FLUIDIC CHANNEL

A Thesis
Presented for the
Master of Science
Degree
The University of Tennessee, Knoxville

Michael Francis Kirsch
December 2002

Dedication

This thesis is dedicated to my family and friends who have always supported me in everything I chose to do. Without their help and encouragement I would never have been able to make it as far as I have. I would especially like to dedicate this to my parents Steve and Lorraine Kirsch who gave me everything and more and instilled in me the drive to seek out and explore.

Acknowledgments

I must first acknowledge my gratitude to my advisor, Dr. Basil Antar for his invaluable help in completing this project. I am also grateful for all the assistance Dr. Kimble gave me with the mathematics. I would like to acknowledge the assistance of Dr. Mark Steven Paley of NASA Marshall Space Flight Center. Dr. Paley provided the setup and description of the experiment along with the motivation behind the research. Acknowledgement would also like to be made to the Tennessee Space Grant Consortium for financial support of this project.

Abstract

The purpose of this research is to determine how long a micro-channel could be in the production of Non-Linear Optical Thin Film Wave-Guides. In determining this length, it is necessary to compute the monomer diffusion process between two solutions of monomers in a micro channel flow. Two models of this flow were created, the first with no flow in a one dimensional channel making diffusion a function of time and position and the second of flow in a two dimensional channel with an imposed velocity profile. Using these models it was determined that the micro channel could be the longest if there was an imposed velocity profile. This velocity caused the forced convection process to dominate over pure diffusion. The simple model can be easily computed and plotted. Unfortunately the complex model requires the solution of a partial differential equation that is not easily solvable using the technique of separation of variables. This technique requires the numerical solution of an eigenfunction problem through the method of Finite Elements and the determination of the coefficients in a Fourier series. The numerical solution is found using the computer programs Mathematica and MatLab. Using these techniques the concentration of monomers was determined throughout the micro channel for both models.

Table of Contents

List of Figures

List of Tables

Nomenclature

A = Fourier Constant

C = Concentration of Monomer

d = Ordinary Derivative

D = Coefficient of Diffusion

E = Eigenvector

h = Height of Channel

k = Constant of Integration

L = Length of Channel

m = integer

M_{ij} = Mass Matrix

n = Integer

N = Number of Nodes

p = Pressure

S_{ij} = Stiffness Matrix

t = Time

u = x Component of Velocity

v = y Component of Velocity

$\vec{v}$ = Velocity Vector

w = Nodal Spacing

x = x Coordinate Position

X = Function of x alone from Separation of Variables

y = y Coordinate Position

Y = Function of y alone from Separation of Variables

Greek

∂ = Partial Derivative

λ = Eigenvalue

μ = Viscosity

φ = Trial Function

ρ = Density

Subscripts

s = Scale Variable

0 = Initial Value of Variable

i = Integer, index of Variable

j = Integer, index of Variable

n = Integer, index of Variable

Superscripts

* = Non-Dimensional Variable

′ = Shorthand for Ordinary Derivative

Chapter 1: Introduction

This research is motivated by the ever-growing importance of high-speed communication in modern society. Light can travel much faster than any other electronic transmission method currently in use and thus is the preferred method. The light must be carried by some medium so that it can reach its desired destination, since it always travels in a straight line. Currently fiber optic cabling is used for carrying signals over long distances. The computer industry would love to take advantage of the major speed advantages of optical data transmission, but as of yet has been unable to. The reason is that current fiber optic techniques are not small enough to be effective for computer applications.

Computers and other electronic devices currently use printed circuit boards that have copper traces for carrying signals through the circuit. Current circuit boards are fast approaching a speed limit with their current design, but new technology is always emerging. If a method could be found to replace copper traces with optical ones then a revolution in computer speed would be upon us.

Another big drawback to copper trace circuit boards is that large amounts of shielding or hardening must be done before a system can be used in space. In space the ambient radiation environment is such that an unprotected circuit board would either burn out or pick up so much interference and noise that it would be useless. An optical circuit board would not have this problem and as such is very promising to the space industry. An optical computer system could reduce costs and weights on future space components since the heavy shielding will no longer be necessary.

The techniques for producing copper trace circuit boards are well known and lend themselves easily to mass production. This leads to low costs and along with the advent of surface mounting techniques very small and compact packages. Since optical tracing is a new concept the techniques for producing them are not yet available and research must be done. The optical traces must be able to be massed produced and be of the same size or smaller than their copper cousins.

The optical traces can be manufactured from thin film optical wave-guides. NASA is presently engaged in development of techniques for producing non-linear optical thin films which can be used for the purpose of manufacturing the wave-guides. NASA is currently producing thin films through the process of photo-deposition.

At NASA Marshall Space Flight Center (MSFC) extensive research has been done into the photo-deposition process. The novel techniques for producing thin films through polymerization have been investigated and some examples of films produced are in *Figures 1-1*.

These figures show good examples of what can be done with the polymerization techniques developed at NASA MSFC. They were produced in quiescent fluids using an apparatus like that sketched in *Figure1- 2*.

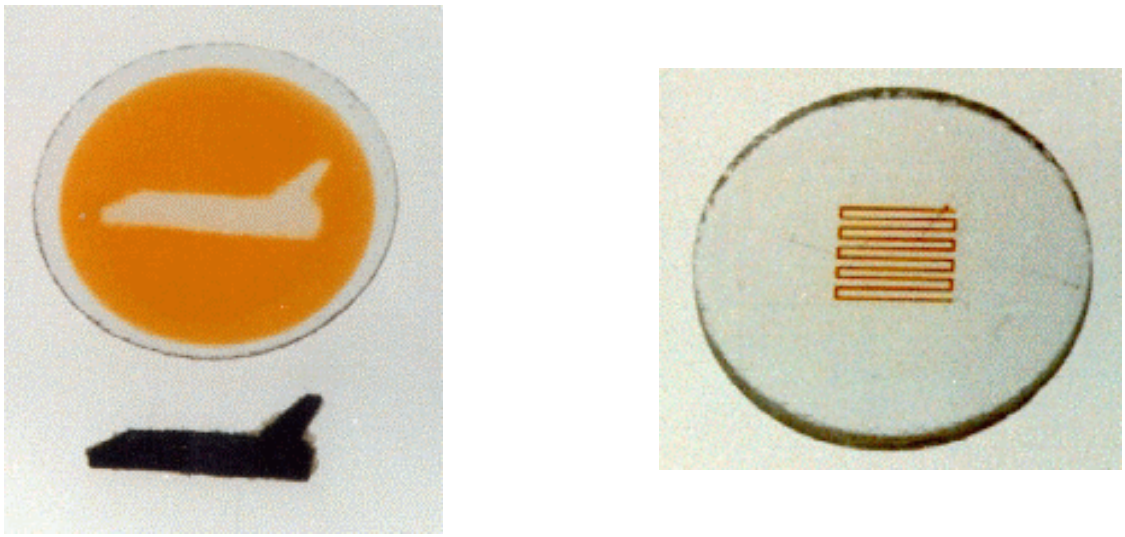

Figure 1-1: Examples of Films Produced using NASA MFSC Photo-deposition Techniques

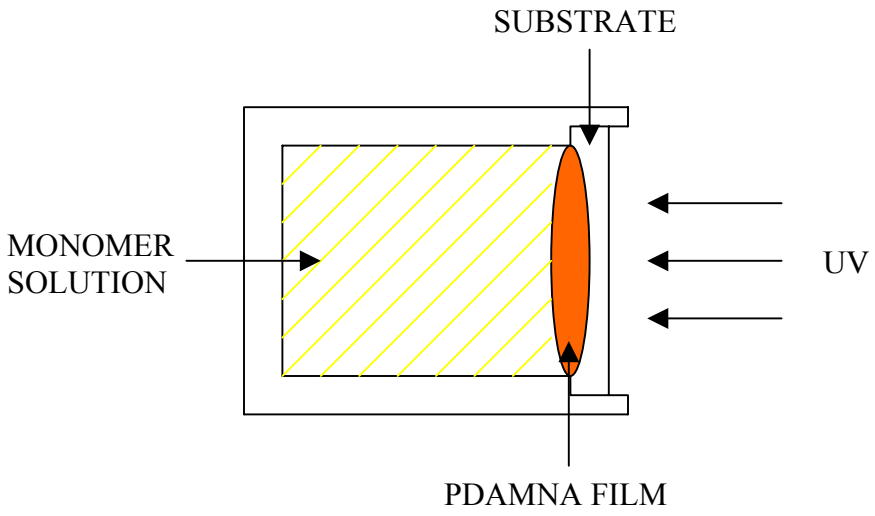

Figure 1-2: Schematic of Apparatus used by NASA MSFC to Create Thin Films

Through the research at NASA MSFC much has been learned about the photo-deposition process; including the kinetics and mechanism of the process, as well as the effects of heat and mass transport. From the research it has been found that the UV radiation becomes attenuated because of absorption by the growing film. It was also found that the rate of film growth during the photo-deposition process varies linearly with light intensity and as the square root of monomer concentration. For this reason the monomer concentration throughout the micro-channel is important.

One technique for replacing copper traces on circuit boards with optical traces is to use non-linear optical thin film wave-guides. The creation of Non-linear Optical Wave-Guides is accomplished through the polymerization of diacetylene monomers (DAMNA) through exposure to an ultraviolet (UV) source. When exposed to UV the monomer undergoes the process of polymerization and the polymeric diacetylene (PDAMNA) film is deposited on a substrate thus producing the wave-guide. The optical wave-guides produced have a very large aspect ratio; see *Figure 1-3*. This means that the wave-guide is extremely long on the order of centimeters and the width is very narrow in relation, on the order of micrometers.

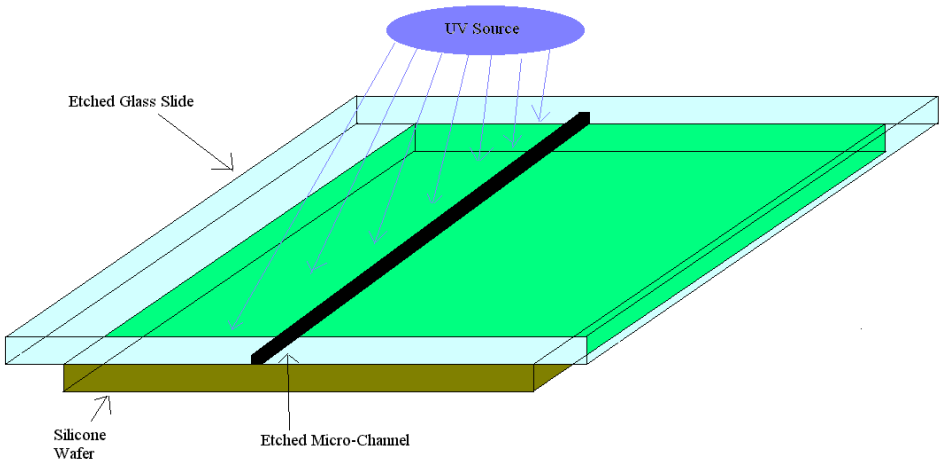

Figure 1-3: Schematic of Apparatus for Wave-Guide Production

Scientists at NASA MSFC have pioneered techniques for the production of these wave-guides. To do this a narrow rectangular channel is etched onto one surface of a quartz substrate, a microscope slide, which is placed atop a silicone wafer; see *Figure 1-3*. Next two different liquids, one a solution starting at one hundred percent concentration and the other a solvent at zero concentration, are forced to flow one atop the other with equal flow rates. This system of flowing liquids is then exposed to a UV source from the upper surface which causes the monomer to polymerize. As the fluids flow down the channel a monolayer of polymer is deposited on the silicone wafer creating the wave-guide. A schematic of the device used by NASA is in *Figure 1-4*.

One of the big questions for creating circuit boards is how long can an optical trace be before the quality of the polymer degrades to the point that it is no longer sufficient? Is there a limit to the type of tracings that can be created and if so what are they? The main parameter here is the length that a trace can be made and still be of high enough quality to be useful. As the monomer diffuses into the solvent eventually there is a high enough concentration that it will begin to polymerize. Once this begins the polymer starts to deposit on the upper surface as well. This deposit quickly grows and

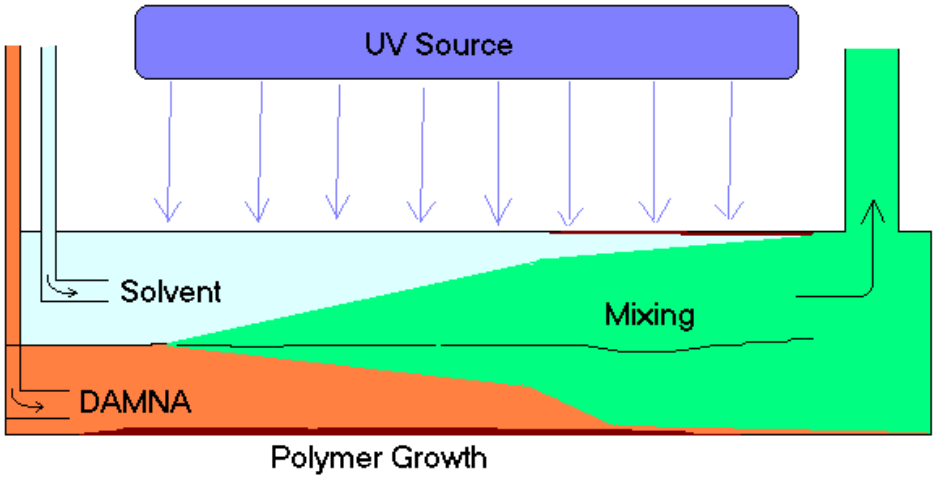

Figure 1-4: Schematic of Apparatus for Producing Optical Wave-Guides

blocks the UV from reaching the monomer near the bottom and the polymerization slows and stops on the bottom surface. This is the end of the useful length of the wave-guide and as such is the main interest of this research. This information will be useful to circuit designers especially when they are laying out the circuit boards.

This research created a numerical model of the diffusion process that takes place within the micro channel flow. The model will be used in determining the length before polymerization of solution stops due to diffusion of solution into solvent and a reaction begins in the solvent. The determined length is then defined as the length before the concentration level reaches a specified value of fifty percent.

This research lays the groundwork for ground based proof of concept testing, done at NASA Marshall Space Flight Center (MSFC). After Ground experiments are run, and results compared with numerical models, experiments will be run in microgravity to produce higher quality Optical Thin Films. Higher quality films can be produced in micro-gravity (μg) due to suppression of fluid flow convection, which can lead to imperfections that affect the quality of the wave-guide produced. The suppression of convection leads to slower diffusion and therefore longer lengths before the concentration drops to fifty percent.

Chapter 2: Mathematical Modeling

In order to determine how long of a wave-guide we can create, the concentration of monomer within the micro channel must be found as a function of position. The determined length is the length at which the concentration decreases to fifty percent. The fluid flow within the micro-channel like all fluid dynamics problems is governed by the fluid flow equations representing conservation of mass, momentum and species. In this case we have incompressible flow so the mass and momentum equations reduce to the Navier-Stokes equations [5]. The concentration of monomers can be modeled using the concentration equation [1].

$$\begin{aligned} &\nabla \cdot \vec{\mathrm{V}} = 0 \\ &\frac{\partial \vec{\mathrm{V}}}{\partial t} + \vec{\mathrm{V}} \cdot \nabla \vec{\mathrm{V}} = -\frac{1}{\rho}\nabla P + \frac{\mu}{\rho}\nabla^2 \vec{\mathrm{V}} \\ &\frac{\partial C}{\partial t} + \vec{\mathrm{V}} \cdot \nabla C = D\nabla^2 C \end{aligned} \tag{2-1}$$

Where $\vec{\mathrm{V}}$ is the fluid velocity, P is the pressure, C is the concentration of monomers, D is the diffusion coefficient, μ is the viscosity of the fluid, and ρ is the density.

These equations are three dimensional and time dependant. They must be solved subject to the initial conditions as well as the boundary conditions that are based upon the geometry of the micro channel. The channel under consideration is of rectangular cross section, four centimeters long by one hundred micrometers high by four hundred micrometers wide. The fluid flow within the channel starts with two layers. These layers are made of solutions with different concentrations of monomers. The bottom layer starts at one hundred percent concentration of monomer, i.e. the solvent is saturated with solute. The top layer begins with zero percent monomer, i.e. no solute in the solvent. The Geometry of the Micro-Fluidic Channel Flow can be seen in *Figure 2-1*. In order to solve the concentration equation, a series of assumptions must be made in order to simplify the equation and make it solvable. Two different sets of assumptions will be made in

modeling the problem. The first model will be for the simple case of diffusion in one dimension with no bulk fluid velocity. The second will be a more complex case for two-dimensional diffusion with an assumed velocity profile.

Model One

For this case, a series of assumptions are made. To begin it is assumed that the fluid is quiescent, i.e. has no fluid velocity components, $\vec{V} = 0$. This means that any term that has velocity in *Equation 2-1* may be neglected; this reduces the equations considerably to the following form:

$$\frac{\partial C}{\partial t} = D\nabla^2 C \tag{2-2}$$

The second assumption is that of an infinite channel, i.e. x and z extend to infinity; in other words that the flow is one-dimensional. This means that in Cartesian coordinates all components with derivatives with respect to the x and z directions are zero. From these assumptions the concentration becomes only a function of time and y position. The concentration equation for this simple model along with its associated boundary and initial conditions is as follows:

$$\frac{\partial C}{\partial t} = D\frac{\partial^2 C}{\partial y^2}$$

$$\frac{\partial C(t,0)}{\partial y} = 0.0 \tag{2-3}$$

$$\frac{\partial C(t,h)}{\partial y} = 0.0$$

$$C(0,y) = \begin{cases} 0 & h/2 \le y \le h \\ C_0 & 0 \le y \le h/2 \end{cases}$$

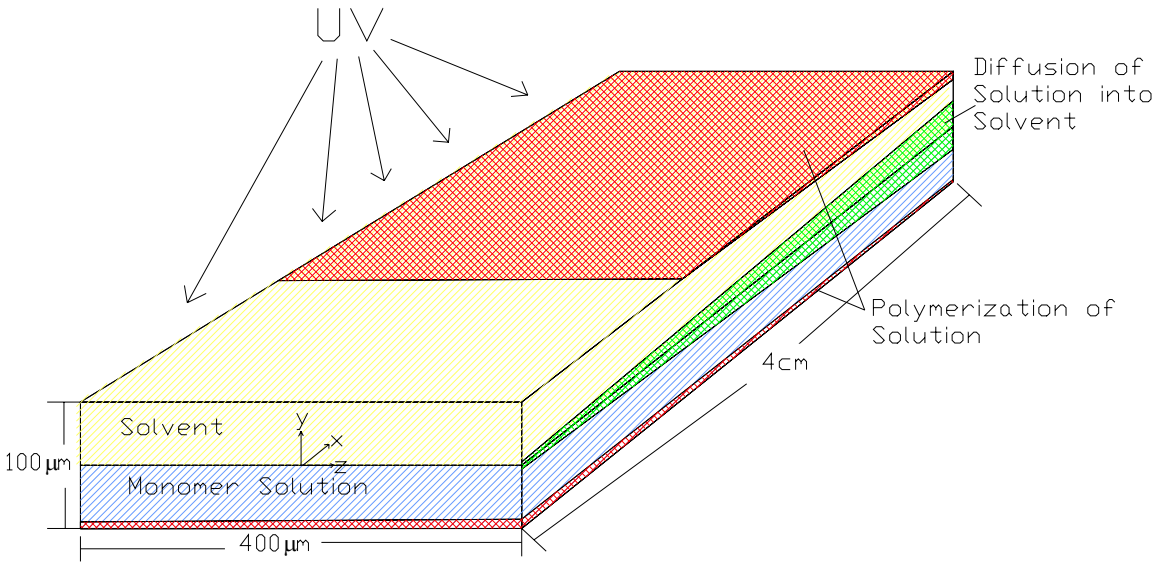

Figure 2-1: Geometry of Micro-Fluidic Channel Flow

A common practice in engineering is to non-dimensionalize the variables. This has the advantage of making the equation and its solution independent of the unit system. It also rescales variables to go between zero and one; this makes it possible to change the scale of the geometry without necessitating the complete resolving of the equations. The variables in the equation will be non-dimensionalized in the following manner:

$$\begin{aligned} y^* &= \frac{y}{h} \\ t^* &= \frac{tD}{h^2} \\ C^* &= \frac{C}{C_0} \end{aligned} \tag{2-4}$$

Applying these variables to the equation simplifies it to:

$$\frac{\partial C^*}{\partial t^*} = \frac{\partial^2 C^*}{\partial y^{*2}} \tag{2-5}$$

This non-dimensional equation is one that can easily be solved using the technique of separation of variables. To do this the concentration which is a function of y and t will be assumed to take the form, $C^*(y^*, t^*) = \mathrm{Y}(y^*)\mathrm{T}(t^*)$. This is then substituted into *Equation 2-5*, and divided by $\mathrm{Y}(y^*)\mathrm{T}(t^*)$ yielding:

$$\frac{1}{T}\frac{\partial T}{\partial t^*} = \frac{1}{Y}\frac{\partial^2 Y}{\partial y^{*2}} = -\lambda^2 \tag{2-6}$$

Since each term is only a function of one variable they can be solved independently of each other. The time equation is:

$$\frac{dT}{dt^*} = -\lambda^2 T \tag{2-7}$$

which by direct integration the is:

$$T(t^*) = ge^{-\lambda^2 t} \tag{2-8}$$

The second equation, y variable, is:

$$\frac{d^2Y}{dy^{*2}} + \lambda^2 Y = 0 \tag{2-9}$$

which can also be integrated and is of the form:

$$Y(y^*) = B\sin(\lambda\, y^*) + K\cos(\lambda\, y^*) \tag{2-10}$$

subject to the following boundary conditions:

$$\begin{aligned} \frac{dY(0)}{dy^*} &= 0 \\ \frac{dY(1)}{dy^*} &= 0 \end{aligned} \tag{2-11}$$

Upon applying the boundary condition at y*=0 it is found that the constant B is equal to zero. Applying the second condition, y*=1, it is found that the condition is only true for specific values of λ. These values are any integer multiple of pi, therefore the second term is:

$$\begin{aligned} &Y_n(y^*) = K_n \cos(\lambda_n y^*) \\ &\lambda_n = n\pi \\ &n = 0,1,.....\infty \end{aligned} \tag{2-12}$$

The concentration can then be found by multiplying together the two components, and since the y equation is dependant on n, must be summed over n. Combining the two constants into a single one, the equation becomes:

$$C^*(y^*,t^*) = \sum_{n=0}^{\infty} K_n \cos(n\pi y^*) e^{-\lambda^2 t} \tag{2-13}$$

To solve for the final constant the initial condition is applied. This can be achieved by multiplying both sides of *Equation 2-13* by an orthogonal eigenfunction and integrating as follows:

$$\int_0^{1/2} C^*(0,y^*)\cos(n\pi y^*)dy^* + \int_0^{1/2} C^*(0,y^*)\cos(n\pi y^*)dy^* = K_n \int_0^1 \cos^2(n\pi y^*)dy^* \tag{2-14}$$

Pulling out the n=0 term gives $K_0 = ½$. Then Integrating and solving for K_n yields:

$$K_n = \frac{2}{n\pi}\sin(\frac{n\pi}{2}) \tag{2-15}$$

Putting everything together the final equation for the concentration in the quiescent fluid as a function of time and height, y, is:

$$C^*(y^*,t^*) = \tfrac{1}{2} + \sum_{n=1}^{\infty} \frac{2}{n\pi}\sin(\frac{n\pi}{2})\cos(n\pi y^*) e^{-n^2\pi^2 t^*} \tag{2-16}$$

Velocity Modeling

The Navier-Stokes equations, *Equation 2-1*, are inherently difficult to solve when there is a nonzero fluid velocity. This difficulty is a result of the nonlinearity of the convection term within the momentum equation. In order to make the equations tractable

an assumption must be made for the velocity profile within the flow. There are many ways to approximate the velocity profile within a duct. Transforming the momentum and mass conservation equations into Cartesian coordinates yields:

$$\begin{aligned}
&\frac{\partial u}{\partial x}+\frac{\partial \mathrm{v}}{\partial y}+\frac{\partial w}{\partial z}=0\\
&u\frac{\partial u}{\partial x}+\mathrm{v}\frac{\partial u}{\partial y}+\mathrm{w}\frac{\partial u}{\partial z}=-\frac{1}{\rho}\frac{\partial P}{\partial x}+\frac{\mu}{\rho}\left[\frac{\partial^2 u}{\partial x^2}+\frac{\partial^2 u}{\partial y^2}+\frac{\partial^2 u}{\partial z^2}\right]\\
&u\frac{\partial \mathrm{v}}{\partial x}+\mathrm{v}\frac{\partial \mathrm{v}}{\partial y}+\mathrm{w}\frac{\partial \mathrm{v}}{\partial z}=-\frac{1}{\rho}\frac{\partial P}{\partial y}+\frac{\mu}{\rho}\left[\frac{\partial^2 \mathrm{v}}{\partial x^2}+\frac{\partial^2 \mathrm{v}}{\partial y^2}+\frac{\partial^2 \mathrm{v}}{\partial z^2}\right]\\
&u\frac{\partial \mathrm{w}}{\partial x}+\mathrm{v}\frac{\partial \mathrm{w}}{\partial y}+\mathrm{w}\frac{\partial \mathrm{w}}{\partial z}=-\frac{1}{\rho}\frac{\partial P}{\partial z}+\frac{\mu}{\rho}\left[\frac{\partial^2 \mathrm{w}}{\partial x^2}+\frac{\partial^2 \mathrm{w}}{\partial y^2}+\frac{\partial^2 \mathrm{w}}{\partial z^2}\right]
\end{aligned} \tag{2-17}$$

Beginning with the equations in Cartesian coordinates, see *Figure 2-2*, and assuming fully developed flow, another assumption can be made that the velocity components, v, w, are zero. Fully developed flow implies that there is no change in velocity in the axial direction, i.e. the partial derivative of any velocity component with respect to x is zero. This assumes that we neglect any entrance region. From this assumption it can be immediately shown that as a consequence of the continuity equation that the u component is independent of x, and only a function of y and z. From this all of the difficult convection terms become zero. Upon substituting this assumption into *Equation 2-2*, the momentum equations become:

$$\begin{aligned}
&0=-\frac{1}{\rho}\frac{\partial P}{\partial x}+\frac{\mu}{\rho}\left[\frac{\partial^2 u}{\partial y^2}+\frac{\partial^2 u}{\partial z^2}\right]\\
&0=-\frac{1}{\rho}\frac{\partial P}{\partial y}\\
&0=-\frac{1}{\rho}\frac{\partial P}{\partial z}
\end{aligned} \tag{2-18}$$

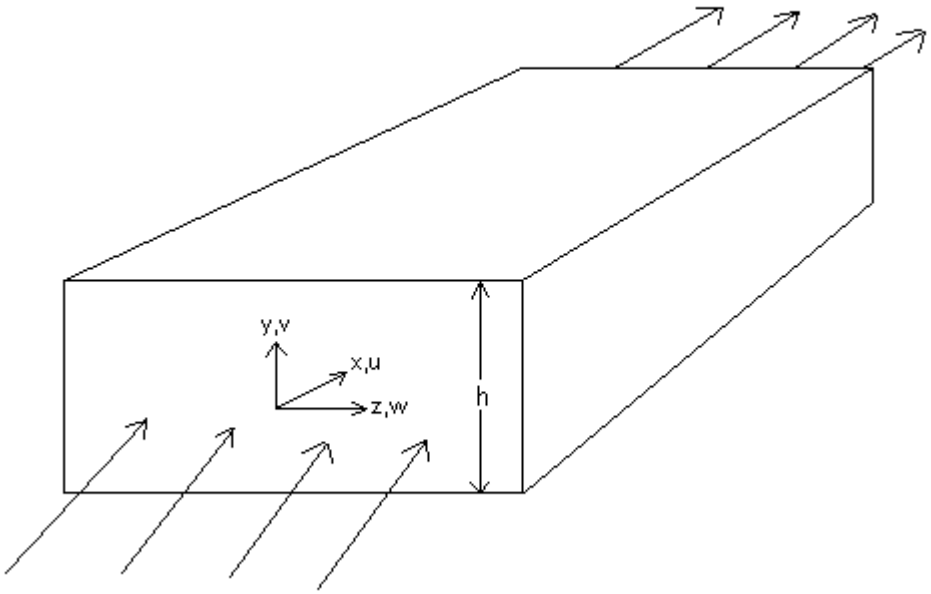

Figure 2-2: Cartesian Coordinates in Duct Flow

If the above y or z momentum equations are integrated it can be seen that the pressure is only a function of x. Also since u is independent of x the pressure gradient must be a constant. This means that the y and z equations are no longer needed and the partial derivative of pressure with respect to x can be changed to an ordinary derivative. Rosenhead [6] gives the solution for this problem for a duct of rectangular cross section as the following series:

$$U(y,z) = \tfrac{1}{2}h^2 - \tfrac{1}{2}y^2 - 2h^2\left(\frac{2}{\pi}\right)^3 \sum_{n=0}^{\infty} \frac{(-1)^n}{(2n+1)^3} \frac{\cosh(2n+1)\left(\pi z/2h\right)}{\cosh(2n+1)\left(\pi c/2h\right)} \cos(2n+1)\frac{\pi y}{2h} \qquad (2\text{-}19)$$

where 2h is the height of the duct measured from the bottom surface. The resulting profile is plotted in *Figure 2-3*. This profile is a paraboloid of revolution and as such has the same cross section throughout. It can be seen that this is an extremely complicated series and therefore further assumptions will be made to make the profile even simpler.

If a further assumption is made that the flow is between two infinite flat plates, representing plane Poiseuille Flow, then the there is no change of velocity in the z direction and the derivative with z becomes zero. This further assumption reduces the momentum equations to:

$$\begin{aligned} 0 &= -\frac{dP}{dx} + \mu\frac{\partial^2 u}{\partial y^2} \\ u(0) &= 0 \\ u(h) &= 0 \end{aligned} \qquad (2\text{-}20)$$

If the pressure gradient is assumed to be a known function then the above equation can be integrated with respect to y. This integration yields an equation with two constants of integration, which must be evaluated from the boundary conditions. For our geometry, see *Figure 2-2*, the equation for the velocity profile needs only be solved for half of the channel since it will be symmetric about the

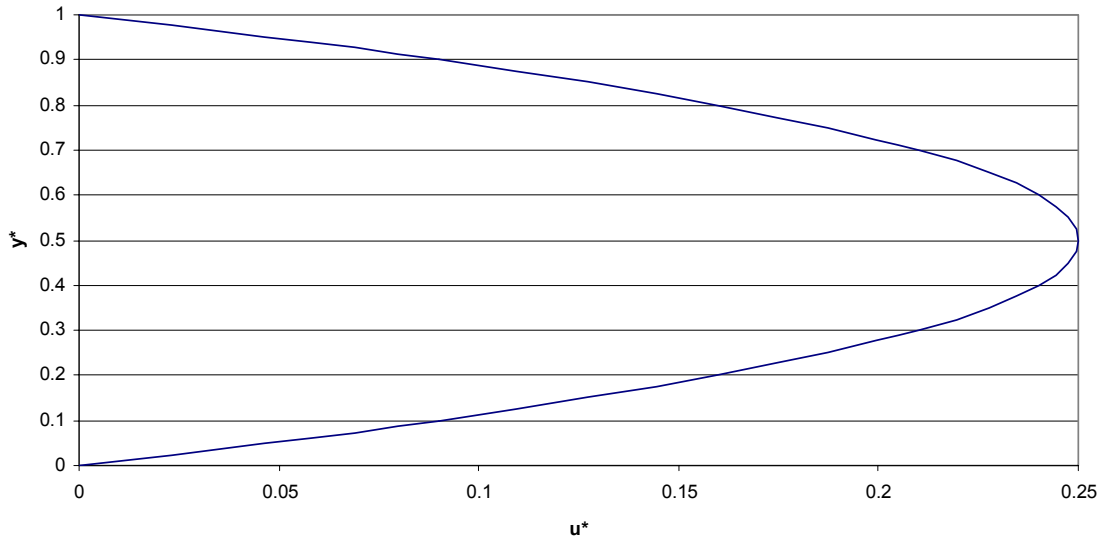

Figure 2-3: Cross Section of the Dimensionless Velocity Profile

centerline. Therefore the profile for the upper half channel is given by the following equation.

$$u = \frac{-h^2}{8\mu}\frac{dP}{dx}\left[1-\left(\frac{y}{h/2}\right)^2\right] \tag{2-21}$$

Since the pressure gradient is assumed known and the geometry is known the velocity profile can be plotted as a function of y alone, *Figure 2-4*.

Model Two

To begin the equations must be stated in our three-dimensional coordinate system based on the geometry of *Figure 2-2*. The conservation equations in Cartesian coordinates take the following form:

$$\begin{aligned}
&\frac{\partial u}{\partial x}+\frac{\partial \mathrm{v}}{\partial y}+\frac{\partial \mathrm{w}}{\partial z}=0\\
&u\frac{\partial u}{\partial x}+\mathrm{v}\frac{\partial u}{\partial y}+\mathrm{w}\frac{\partial u}{\partial z}=-\frac{1}{\rho}\frac{\partial P}{\partial x}+\frac{\mu}{\rho}\left[\frac{\partial^2 u}{\partial x^2}+\frac{\partial^2 u}{\partial y^2}+\frac{\partial^2 u}{\partial z^2}\right]\\
&u\frac{\partial \mathrm{v}}{\partial x}+\mathrm{v}\frac{\partial \mathrm{v}}{\partial y}+\mathrm{w}\frac{\partial \mathrm{v}}{\partial z}=-\frac{1}{\rho}\frac{\partial P}{\partial y}+\frac{\mu}{\rho}\left[\frac{\partial^2 \mathrm{v}}{\partial x^2}+\frac{\partial^2 \mathrm{v}}{\partial y^2}+\frac{\partial^2 \mathrm{v}}{\partial z^2}\right]\\
&u\frac{\partial \mathrm{w}}{\partial x}+\mathrm{v}\frac{\partial \mathrm{w}}{\partial y}+\mathrm{w}\frac{\partial \mathrm{w}}{\partial z}=-\frac{1}{\rho}\frac{\partial P}{\partial z}+\frac{\mu}{\rho}\left[\frac{\partial^2 \mathrm{w}}{\partial x^2}+\frac{\partial^2 \mathrm{w}}{\partial y^2}+\frac{\partial^2 \mathrm{w}}{\partial z^2}\right]\\
&u\frac{\partial C}{\partial x}+\mathrm{v}\frac{\partial C}{\partial y}+\mathrm{w}\frac{\partial C}{\partial z}=D\left[\frac{\partial^2 C}{\partial x^2}+\frac{\partial^2 C}{\partial y^2}+\frac{\partial^2 C}{\partial z^2}\right]
\end{aligned} \tag{2-22}$$

In this model the first assumption is that of a two-dimensional model; therefore all z dependent components are zero. This reduces the conservation equations to the following form.

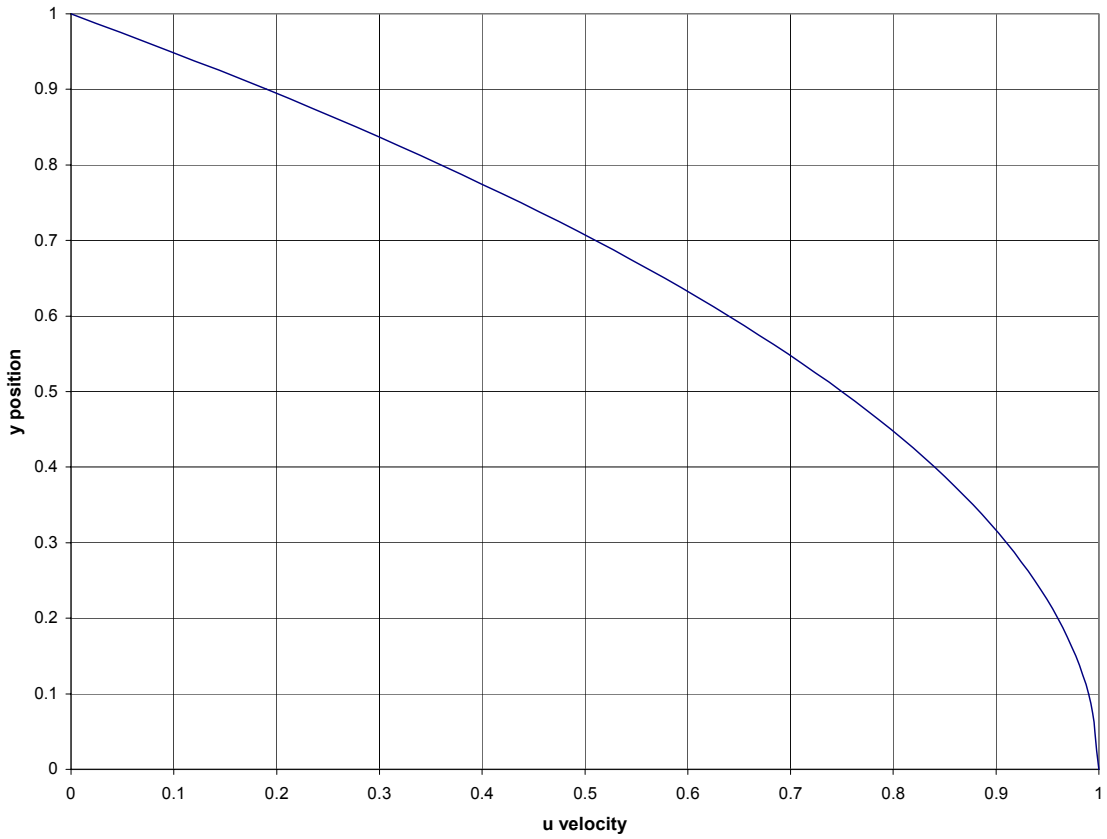

Figure 2-4: Dimensionless Poiseuille Flow Profile for Upper half Channel

$$\frac{\partial u}{\partial x}+\frac{\partial \mathrm{v}}{\partial y}=0$$
$$u\frac{\partial u}{\partial x}+\mathrm{v}\frac{\partial u}{\partial y}=-\frac{1}{\rho}\frac{\partial P}{\partial x}+\frac{\mu}{\rho}\left[\frac{\partial^2 u}{\partial x^2}+\frac{\partial^2 u}{\partial y^2}\right] \tag{2-23}$$
$$u\frac{\partial \mathrm{v}}{\partial x}+\mathrm{v}\frac{\partial \mathrm{v}}{\partial y}=-\frac{1}{\rho}\frac{\partial P}{\partial y}+\frac{\mu}{\rho}\left[\frac{\partial^2 \mathrm{v}}{\partial x^2}+\frac{\partial^2 \mathrm{v}}{\partial y^2}\right]$$
$$u\frac{\partial C}{\partial x}+\mathrm{v}\frac{\partial C}{\partial y}=D\left[\frac{\partial^2 C}{\partial x^2}+\frac{\partial^2 C}{\partial y^2}\right]$$

The second assumption is that of steady flow. Therefore, there is no time dependence. The third assumption is again that of no source term. It will also be assumed that the diffusion in the x direction will be negligible; this is because the forced convection in the x direction is the dominating term. Fourth, we will assume that we can solve the problem for the top half channel since the lower half should be anti-symmetric. With all of these assumption the governing equations reduces to:

$$u\frac{\partial C}{\partial x}=D\frac{\partial^2 C}{\partial y^2} \tag{2-24}$$

The fifth assumption is that the velocity profile can be modeled as plane Poiseuille flow as previously derived. This gives the u component of velocity as a function of y alone and the v component as zero. Restating, the equation for the velocity profile of plane Poiseuille flow is:

$$u=\frac{-h^2}{8\mu}\frac{dP}{dx}\left[1-\left(\frac{y}{h/2}\right)^2\right] \tag{2-25}$$

As in model one, the variables in the concentration equation will be non-dimensionalized; this will be done as follows:

$$
\begin{aligned}
C^* &= \frac{C}{C_0} \\
u^* &= \frac{u}{u_s} \qquad u_s = \frac{-h^2}{12\mu}\frac{dP}{dx} \\
x^* &= \frac{x}{x_s} \qquad x_s = \frac{3}{8}\frac{h^2}{4D}u_s = \frac{-h^4}{128\mu D}\frac{dP}{dx} \\
y^* &= \frac{y}{y_s} \qquad y_s = h/2
\end{aligned}
\tag{2-26}
$$

Substituting these variables along with the velocity profile into *Equation 2-24* gives the non-dimensional form of the concentration equation as:

$$
(1-y^{*2})\frac{\partial C^*}{\partial x^*} = \frac{\partial^2 C^*}{\partial y^{*2}} \tag{2-27}
$$

subject to the following conditions:

$$
\begin{aligned}
C^*(0,y^*) &= \begin{cases} 1 & \tfrac{1}{2} \le y^* \le 1 \\ 0 & 0 \le y^* \le 1 \end{cases} \\
\frac{\partial C^*(x^*,0)}{\partial y^*} &= 0 \\
\frac{\partial C^*(x^*,1)}{\partial y^*} &= 0
\end{aligned}
\tag{2-28}
$$

From this point on in the derivation, all of the asterisk on the variables will be dropped, but all remain non-dimensional; this is done for ease of writing. Again, the technique of separation of variables (SOV) will be employed; unfortunately it is not as simple as in model one. For SOV, it will be assumed that the concentration can be written as C(x,y)=X(x)Y(y). Putting this into the concentration equation and dividing by C the equation becomes:

$$\frac{1}{X}\frac{dX}{dx} = \frac{1}{(1-y^2)}\frac{1}{Y}\frac{d^2Y}{dY^2} = -\lambda^2 \tag{2-29}$$

The only way in which a function of x alone can be equal to a function of y alone is if they are equal to a constant. That constant will be assumed to be $-\lambda^2$. Since each of these equations is an ordinary differential equation and equal to a constant, they can be integrated. The X equation is given by:

$$\frac{dX}{dx} = -\lambda^2 X \tag{2-30}$$

which can be easily solved and is given as:

$$X(x) = ke^{-\lambda^2 x} \tag{2-31}$$

The Y equation is:

$$\begin{aligned} &Y'' + \lambda^2\left(1-y^2\right)Y = 0 \\ &Y(0) = 0 \\ &Y'(1) = 1 \end{aligned} \tag{2-32}$$

The general solution of which is:

$$Y(y) = A_1E_1(y) + A_2E_2(y) \tag{2-33}$$

where E_1 and E_2 are linearly independent solutions. Unfortunately, these solutions are not easily computed. Therefore we will have to come up with another method for solving our eigenfunction problem. The eigenfunction problem problems definition is not complete unless it has both the differential equation and the boundary conditions. The differential

equation is one dimensional, second order and homogenous. The boundary conditions are mixed with one essential (Dirichlet) boundary condition and one natural (Neumann).

This differential equation has been solved with different boundary conditions by a number of different researchers. Sparrow et al [7] solved the equation for two cases, one with the Y(1) = 0 and dY/dy(0) = 0, and the other for dY/dy = 0 for y = 0,1. Although similar, neither of these conditions satisfies our equation. Therefore we will need to solve for the eigenvalues and eigenfunctions ourselves. This will be a major topic of chapter 3.

Once the eigenfunction problem is solved the results can be used to find the solution for the concentration at any position within the micro-channel. The results are put into the following equation for the concentration, which was found through separation of variables, after the boundary conditions are satisfied.

$$C_n(x,y) = \sum_{n=1}^{\infty} A_n E_n(y) e^{-\lambda_n^2 x} \tag{2-34}$$

Our problem is a "Regular Sturm-Liouville" problem [4], for which the standard form of the equation and boundary conditions are:

$$\begin{aligned} &\frac{d}{dy}\left(p(y)\frac{d\phi}{dy}\right) + q(y)\phi + \lambda\sigma(y)\phi = 0 \\ &\beta_1\phi(a) + \beta_2\frac{d\phi}{dy}(a) = 0 \\ &\beta_3\phi(b) + \beta_4\frac{d\phi}{dy}(b) = 0 \end{aligned} \tag{2-35}$$

and as such has all of its properties, Haberman [4]. For our problem the coefficients in the standard equation are:

$$p(y)=1 \quad q(y)=0 \quad \sigma(y)=(1-y^2)$$
$$a=0 \quad \beta_1=1 \quad \beta_2=0 \quad \phi(a)=0 \quad \frac{d\phi}{dy}(a)=0 \tag{2-36}$$
$$b=0 \quad \beta_3=0 \quad \beta_4=1 \quad \phi(b)=0 \quad \frac{d\phi}{dy}(b)=1$$

The most important property of the "Regular Sturm-Liouville" problem is that all of the eigenfunctions are orthogonal. The eigenfunctions are orthogonal if and only if:

$$\int_0^1 (1-y^2)E_n(y)E_m(y)dy = \begin{cases} 0, & n \neq m \\ \text{non-zero-constant} & n=m \end{cases} \tag{2-37}$$

Because of the orthogonality condition the standard method for finding the constant A_n can be employed. This involves multiplying the equation for C(0,y) by $(1-y^2)E_n(y)$ and integrating and applying the initial condition on x. The initial condition on x states that the concentration at x=0 is 1 and therefore solving for the Fourier constant, A_n, yields:

$$A_n = \frac{\int_0^1 (1-y^2)E_n(y)dy}{\int_0^1 (1-y^2)E_n^2(y)dy} \tag{2-38}$$

Chapter 3: Results and Discussion

Having mathematical models of the physics of our problem it is now time to come up with methods of computing the value of the concentration within the micro-channel. The solution for each of the models requires employment of numerical techniques.

Solution for Model One

The derivation of the first model provided an analytic solution in the form of an infinite series, *Equation 2-16*.

$$C^*(y^*,t^*) = \frac{1}{2} + \sum_{n=1}^{\infty} \frac{2}{n\pi} \sin\left(\frac{n\pi}{2}\right) \cos(n\pi y^*) e^{-n^2\pi^2 t^*} \tag{2-16}$$

From inspection of this equation it can easily be seen that the diffusion field is only a function of time and height within the channel, i.e. y position. This means that given values at y and t the concentration can be readily determined provided one can perform a summation over infinity.

Since it is not possible to take an infinite number of terms in the Fourier series, a finite number had to be computed. For any time greater than zero the series can be cut off at a finite number of terms. This is due to the fact that the magnitude of an individual element approaches zero. This was determined by incrementally increasing the number of terms. The number of terms was steadily increased until one hundred terms were used. At one hundred terms the value of an individual element is on the order of 10^{-61} or smaller, which for all practical purposes is zero.

Since the concentration can only be found for a point where we know its coordinates, the region is broken down into a series of points along the length of the channel. The concentration can then be computed for each of these points at series of time steps. Using Microsoft Excel the concentration was computed at each x and t point, which was then plotted, *Figure 3-1*.

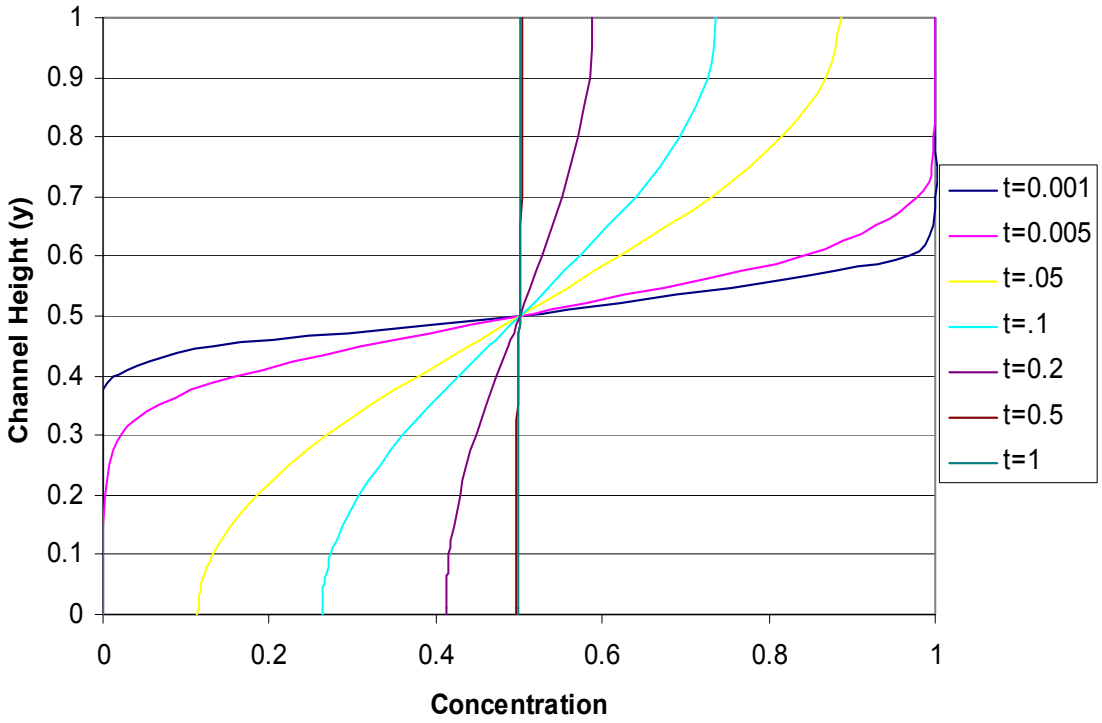

Figure 3-1: Model 1 Dimensionless Concentration as a Function of Non-Dimensional Channel Height and Time

This plot allows for the visualization of the monomer concentration field within the quiescent micro-channel. From inspection it can easily be seen that as expected the concentration level tends toward equilibrium over long time. This plot also makes it possible to answer our primary question, of how long of wave-guide can be produced. Since our main criteria for judgment was the time before concentration became fifty percent, a contour plot of the concentration within the micro-channel was created, *Figure 3-2*. The time before concentration dips to fifty percent can be seen to be 0.5.

Solution for Model Two

The concentration in this model is a function of the fluid velocity field. Since this velocity field was part of the differential equation, the only thing needed to find the concentration at a point is the coordinates of that point. Unfortunately the solution of the differential equation in this model is not as straightforward as in the previous one. Since the eigenfunction equation in y could not be solved, a numerical solution method had to be used.

Restating the problem the non-dimensional partial differential equation for the concentration is:

$$(1-y^{*2})\frac{\partial C^*}{\partial x^*}=\frac{\partial^2 C^*}{\partial y^{*2}} \tag{2-27}$$

The eigenfunction problem with its associated boundary conditions is:

$$\begin{aligned} &Y''+\lambda^2\left(1-y^2\right)Y=0 \\ &Y(0)=0 \\ &Y'(1)=1 \end{aligned} \tag{2-33}$$

The final solution will be a series of the form:

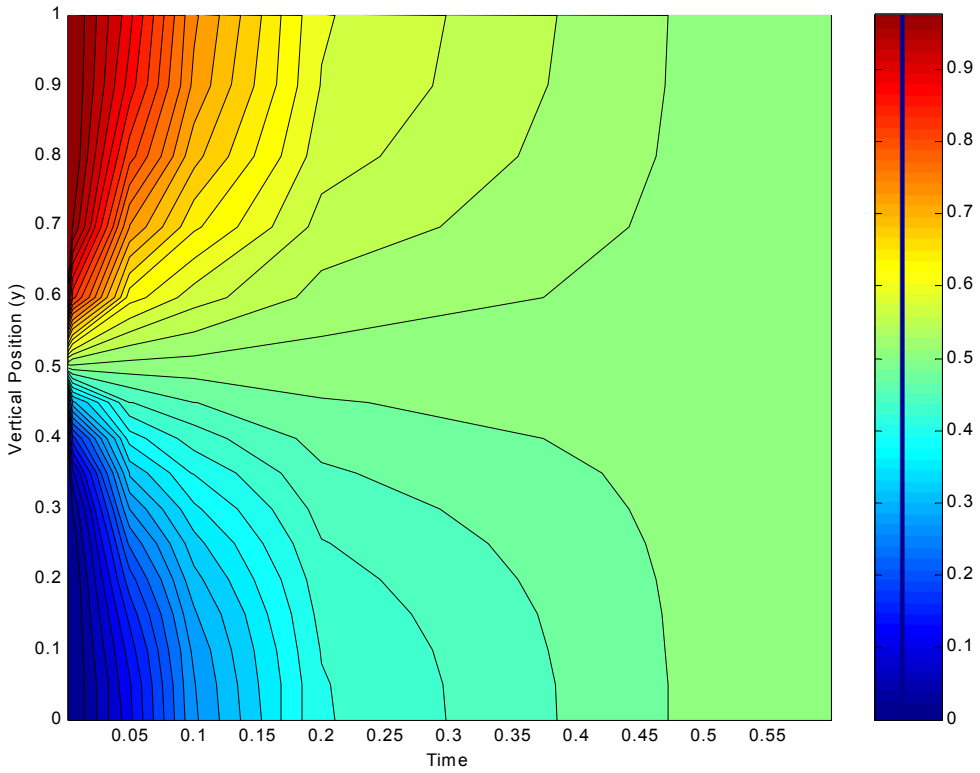

Figure 3-2: Contour Plot of Model 1 Dimensionless Concentration as a Function of Non-Dimensional Position and Time

$$C_n(x,y) = \sum_{n=1}^{\infty} A_n E_n(y) e^{-\lambda_n^2 x} \tag{2-34}$$

There are many ways to go about solving an eigenfunction problem numerically. One method is the use of a numerical integrator like Mathematica's 'NDSOLVE'. Unfortunately the equation is exceptionally stiff and the boundary conditions could not be met with this technique. A second technique is the method of series solution, also known as the method of Frobenius [2], where the solution is represented by an infinite polynomial and the coefficients are found from a recursion relation. To produce this series solution it is assumed that the solution of the eigenfunction problem can be represented as a series:

$$\begin{aligned} Y(x) &= \sum_{n=0}^{\infty} a_n x^n \\ Y'(x) &= \sum_{n=0}^{\infty} n a_n x^{n-1} \\ Y''(x) &= \sum_{n=0}^{\infty} n(n-1) a_n x^n \end{aligned} \tag{3-1}$$

By substituting these series into the differential equation for the eigenfunction problem, *Equation 2-32*, and applying the boundary conditions a solution of the eigenfunction problem can be found by summing up all the terms of the solution over position. To find each term in the series a recursion relation is needed. This relation is found by the making the power of x the same for each, collecting all the terms under one summation, and solving for a_n.

$$a_n = \frac{\lambda^2}{n(n-1)}\left(a_{n-4} - a_{n-2}\right) \tag{3-2}$$

This relation shows that as long as the previous terms in the series are known the next term can be calculated. From the boundary conditions the first few terms can be found for the series and they are:

$$\begin{aligned} a_0 &= 0 \\ a_1 &= 1 \\ a_2 &= 0 \\ a_3 &= -\frac{\lambda^2}{6} \end{aligned} \tag{3-3}$$

All the terms in the even series are identically zero and all of the terms in the odd series can be determined in terms of a_1 and a_3. These, in turn, can be solved strictly in terms of the eigenvalues, λ^2.

Unfortunately when implementing this technique with our conditions the computer power required was beyond any available. The computer was able to compute a large number of terms in the series before it ran out of memory; even when one hundred terms in the series are retained only the first two eigenvalues could be determined with any precision. *Figure 3-3* shows the series solution as a function of λ using 100 terms in the series expansion. The eigenvalues are determined by locating the points where the graph of the series crosses the x-axis as in *Figure 3-3*.

This technique of series approximation is a well-known brute force technique. It has been used by a number of researchers in solving similar problems. The problems are similar in that they have the same basic partial differential equation but they have different boundary conditions. Cess and Shaffer [3] used this technique in solving the second case of Sparrow et al [7]. Each of these researchers was able to find the first ten eigenvalues or so. The difference in boundary conditions will lead to radically different eigenvalues and eigenfunctions even though the governing equations are identical.

The technique that worked well was the Finite Element Method (FEM) [8]. This method uses a trial function at a number of points in the region to approximate the actual function. The region is broken down into finite intervals,

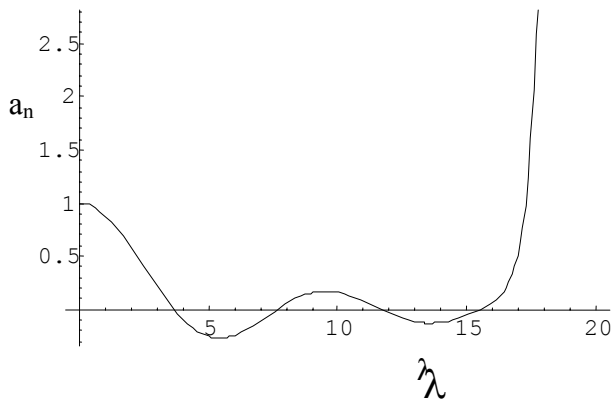

Figure 3-3: Plot of Frobenius Method using 100 terms

or elements. Two nodes or points define each element. Later these nodes will be used as the points where the concentration can be evaluated.

The first thing that must be done is to assume an approximation for Y(y). The solution Y(y) will be approximated by a series with the coefficients being the eigenfunction coefficients multiplying the trial functions, φ_j.

$$Y(y) = \sum_{j=0}^{N} E_j \varphi_j(y) \tag{3-4a}$$

In the above equation j is the number of discrete nodes in the interval [0,1]. The trial functions, φ_j, is chosen such that $\varphi_{j-1} = \varphi_{j+1} = 0$ for all j.

Upon applying the boundary conditions on Y, namely that Y(0)=0 it is found E_0=0. Therefore the first term in the summation is zero and can be dropped so the summation now goes from 1 to N.

$$Y(y) = \sum_{j=1}^{N} E_j \varphi_j(y) \tag{3-4b}$$

Next the differential equation is put into the weak form, see Strang and Fix [8], by taking the inner product of the equation with the chosen trial function. This means multiplying the equation by the trial function and integrating, the equation as follows:

$$0 = \int_0^1 \varphi_j(y)[Y'' + \lambda(1-y^2)Y]dy \qquad j = 1...N \tag{3-5}$$

This equation must be solved along with the boundary conditions and upon integrating by parts once becomes:

$$0 = \varphi_j(y)Y'(y)\Big|_0^1 + \int_0^1 -\varphi_j'(y)Y'(y) + \lambda^2(1-y^2)Y(y)\varphi_j(y)dy \qquad j = 1...N \tag{3-6}$$

Upon applying the boundary conditions, the leading term in the above equation is zero. This is because for all j greater than zero the trial function is zero at y=0 and at y=1 all of the trial functions except j=N are zero, and due to the boundary condition at y=1 that product is also zero. Putting the approximation for Y(y) into the previous equation yields a matrix equation.

$$0 = \sum_{j=1}^{N} E_j \left[\int_0^1 \{-\varphi_i'\varphi_j' + \lambda^2(1-y^2)\varphi_i\varphi_j\}dy \right] \qquad i = 1....N \qquad E_0 = 0 \tag{3-7}$$

Sticking with the convention of the FEM, the matrix equation will be broken up into a stiffness and mass matrix. The stiffness matrix (S_{ij}) is the second term of the equation and the mass matrix (M_{ij}) is the third.

$$S_{m,n} = \int_0^1 -\varphi_i' \varphi_j' dy$$
$$M_{m,n} = \int_0^1 (1-y^2)\varphi_i \varphi_j dy \qquad (3\text{-}8)$$
$$m,n = 1...N$$

The matrix equation now looks relatively simple:

$$(S_{m,n} + \lambda^2 M_{m,n})E_n = 0. \qquad (3\text{-}9)$$

This represents a standard matrix eigenvalue problem and there exist many techniques for its solution. The solution of this matrix equation will then give us our eigenvalues, λ, and eigenfunctions, Y_n.

In order to continue the trial function, φ_n, must be defined. There are many options, piecewise linear, spline, polynomial etc. A piecewise linear trial function that involves three nodes was chosen. This trial function involves the node under consideration plus the one to the left and right of it, see *Figure 3-4*. The function is equal to one at the central node and zero at the left and right node and varies linearly between any two nodes. The equation for this trial function is as follows:

$$\varphi_i(y) = \begin{cases} 1 + \frac{1}{w}(y - kw) & y \le kw \\ 1 - \frac{1}{w}(y - kw) & y \ge kw \end{cases} \qquad (3\text{-}10)$$

where k is the node number, w is the node spacing and y is the position. Also needed is the derivative of the trial function, which is given as:

$$\varphi_i'(y) = \begin{cases} 1/w & y \le kw \\ -1/w & y \ge kw \end{cases} \qquad (3\text{-}11)$$

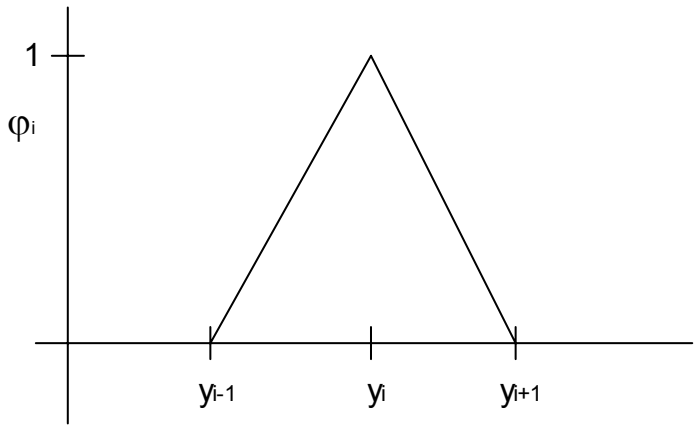

Figure 3-4: Plot of Trial Function

Using this trial function in *Equation 3-8* the mass and stiffness matrices can be determined. Upon substituting the trial functions into the mass and stiffness equations, three basic cases result. These cases result from where the evaluation of the trial function occurs.

For the first case of the mass matrix, if the point is left of the current node, i.e. m=n-1, then it is on the sub-diagonal and has the following equation:

$$M_{n,(n-1)} = \int_{(n-1)w}^{nw} \left(1-y^2\right)\left(1-\frac{1}{w}(y-nw)\right)\left(1+\frac{1}{w}(y-nw)\right)dy \qquad (3\text{-}12)$$

If the point is to the right, m=n+1, the entry is on the super-diagonal and can be found from:

$$M_{n,(n+1)} = \int_{nw}^{(n+1)w} \left(1-y^2\right)\left(1-\frac{1}{w}(y-nw)\right)\left(1+\frac{1}{w}(y-nw)\right)dy \qquad (3\text{-}13)$$

and if the point is at the node, m=n then the entry goes on the diagonal and the equation is:

$$M_{n,n} = \int_{(n-1)w}^{nw} \left(1-y^2\right)\left(1+\frac{1}{w}(y-nw)\right)^2 dy + \int_{nw}^{(n+1)w} -\left(1-y^2\right)\left(1-\frac{1}{w}(y-nw)\right)^2 dy \quad (3\text{-}14)$$

All other terms in the matrix are zero. Therefore the mass matrix contains nonzero entries only on the diagonal, sub-diagonal, and super-diagonal. Because it is a boundary element and it is not possible to have a trial function to its right the last node is slightly different. The last node is at n=N, where N is the total number of nodes in the system. Since it is on the diagonal it should have an equation similar to *Equation 3-14*, but it does not have the second term.

$$M_{N,N} = \int_{(N-1)w}^{Nw} \left(1-y^2\right)\left(1+\frac{1}{w}(y-Nw)\right)^2 dy \qquad (3\text{-}15)$$

The stiffness matrix is considerably easier to calculate. All diagonal elements are two times the number of nodes and all of the super and sub diagonal terms are negative one times the number of nodes. Again the last node is special and it is just the number of nodes.

Since determining each of the matrices requires integration and there are a large number of nodes the computer program Mathematica was used. Using Mathematica each of the matrices could be created and stored in text files. See *Equation A-1* for an example of how to calculate a ten node mass matrix. *Equation A-2* is a similar example of a ten node stiffness matrix. Mathematica code is similar to C++ code except that standard mathematical notation can be used. The input code for the creation of matrices for a six-node system is in *Figure A-1*.

With these matrices it is now possible to solve the matrix equation for the eigenvalues and eigenvectors. The computer program MATLAB, short for Matrix Laboratory, is ideally suited to do just that. With just a few commands MATLAB computes the eigenvalues and eigenvectors and stores them for later use. MATLAB has a built in function 'eig' whose input is two matrices, a mass matrix and a stiffness matrix, and whose output is the eigenvalues and eigenvectors. By loading the matrices that Mathematica calculated into MATLAB and calling 'eig' it has become possible to solve the eigenfunction problem. The commands for solving the eigenfunction problem are in *Figure A-2*.

Next to be found is the Fourier constant. This constant, A_n, can be evaluated by putting the eigenvectors just found into *Equation 2-37*.

$$A_n = \frac{\int_0^1 (1-y^2)E_n(y)dy}{\int_0^1 (1-y^2)E_n^2(y)dy} \tag{2-37}$$

Again, we need to perform integration and therefore Mathematica was used. By importing the eigenvectors from MATLAB to Mathematica it becomes a simple task to perform this integration and find the Fourier constants. The code for doing this is in *Figure A-3*.

We can then finish up with determining the concentration as a function of the x and y position by substituting into the series generated by separation of variables.

$$C_n(x,y) = \sum_{n=1}^{\infty} A_n E_n(y) e^{-\lambda_n^2 x} \tag{2-34}$$

Now that all the necessary components of *Equation 2-34* have been determined it can all be put together to find the concentration as a function of position. As with model one it is not possible to take an infinite number of terms so a finite number must be used. Because of the exponential in the x term only a few terms will need to be taken since the

eigenvalues get large quickly. Twenty terms were used; the value of the exponential of the twentieth term is on the order of 10^{-6000}, which is essentially zero, and therefore contributes little to the summation. Since these operations are really matrix operations, MATLAB was again used, and the commands are in *Figure A-4*. The concentration was found for the upper half channel at each node in the y direction and at values of x ranging from 0.1 to 1.

Since accuracy increases with the number of nodes used, one thousand nodes were used. A thousand nodes were chosen to obtain four place convergence of the eigenvalues. The number of nodes was increased and the eigenvalues calculated until the first twenty converged. In order to illustrate the convergence *Table 3-1* contains the calculated eigenvalues for 10, 50, 100, 500, and 1000 nodes. From this table it can be seen that as the nodes increase the value of any eigenvalues remains essentially constant, i.e. it becomes converged. Therefore the mass and stiffness matrices are one thousand columns by one thousand rows each. This large number of calculations caused the typical time to find a solution to be on the order of six to eight hours.

The eigenfunction problem that was solved here is not completely unique to this application, and therefore some of the results might be useful for other applications. These include the values of the first twenty eigenvalues and constants along with the value of the eigenvector at y equal one. *Table 3-2* contains these results. Also instructive is a plot of a few of the eigenvectors, it is important to have a good idea of their shape. Plots of the second, fifth, tenth, and twentieth eigenvectors are *Figure 3-5, 3-6, 3-7, and 3-8* respectively.

Having the value of the concentration at many points listed in table format would not be very instructive, so in order to visualize things it will be plotted. *Figure 3-9* gives the concentration as a function of x and y positions within the upper half of the micro-channel. A contour plot, *Figure 3-10*, was created to better visualize the variation of the concentration at every point within the micro-channel. Using this figure we can now answer our driving question of wave-guide length. It can be seen that at even a small distance up from the centerline the concentration is above our threshold, of fifty percent, for most of the channel length and asymptotically approaches fifty percent as we get near

Table 3-1: Convergence of First Ten Eigenvalues

	Number of Nodes				
Eigenvalue	10	50	100	500	1000
1	2.279	2.264	2.263	2.263	2.263
2	6.422	6.303	6.299	6.298	6.298
3	10.742	10.325	10.312	10.308	10.308
4	15.373	14.355	14.323	14.313	14.313
5	20.400	18.400	18.337	18.317	18.316
6	25.799	22.467	22.355	22.320	22.318
7	31.231	26.560	26.380	26.322	26.320
8	36.593	30.684	30.412	30.325	30.322
9	47.783	34.845	34.452	34.327	34.323
10	84.869	39.046	38.504	38.330	38.325
11		43.294	42.566	42.333	42.326
12		47.592	46.641	46.337	46.327
13		51.944	50.730	50.341	50.329
14		56.357	54.834	54.345	54.330
15		60.832	58.954	58.350	58.332
16		65.376	63.092	62.356	62.333
17		69.991	67.248	66.363	66.335
18		74.680	71.424	70.370	70.337
19		79.447	75.621	74.378	74.339
20		84.293	79.840	78.387	78.342

Table 3-2: Eigenvectors, Eigenvalues, and Constants for Solution of Eigenfunction Problem.

n	λ_n	A_n	$E_n(1)$
1	2.26311	-0.7256	-1.8443
2	6.2977	-0.2546	2.1424
3	10.3078	-0.1551	-2.3137
4	14.3129	0.11161	-2.4377
5	18.3161	0.08718	2.5361
6	22.3185	-0.0715	2.6184
7	26.3203	-0.0607	-2.6893
8	30.3218	-0.0526	2.7519
9	34.3232	0.0465	2.8081
10	38.3245	0.04164	-2.8592
11	42.3258	0.03771	2.906
12	46.3272	0.03445	-2.9493
13	50.3285	-0.0317	-2.9897
14	54.33	0.02937	-3.0275
15	58.3316	0.02736	3.063
16	62.3333	0.0256	-3.0967
17	66.3352	0.02406	3.1286
18	70.3372	0.02269	-3.1589
19	74.3395	0.02147	3.1879
20	78.3419	0.02037	-3.2156

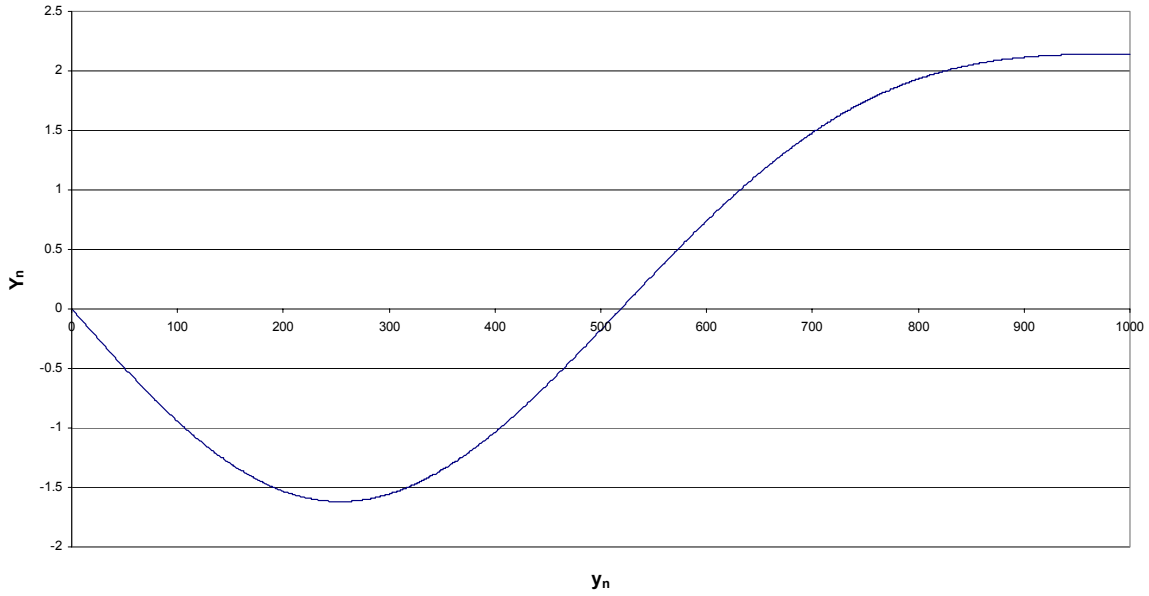

Figure 3-5: Plot of Second Eigenvector

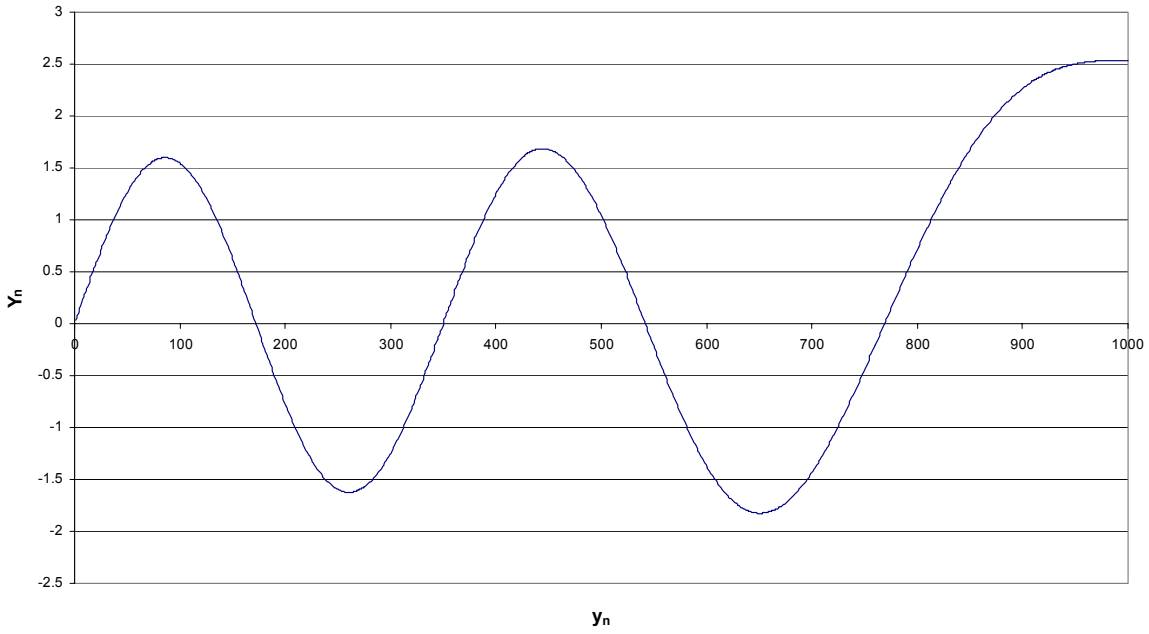

Figure 3-6: Plot of Fifth Eigenvector

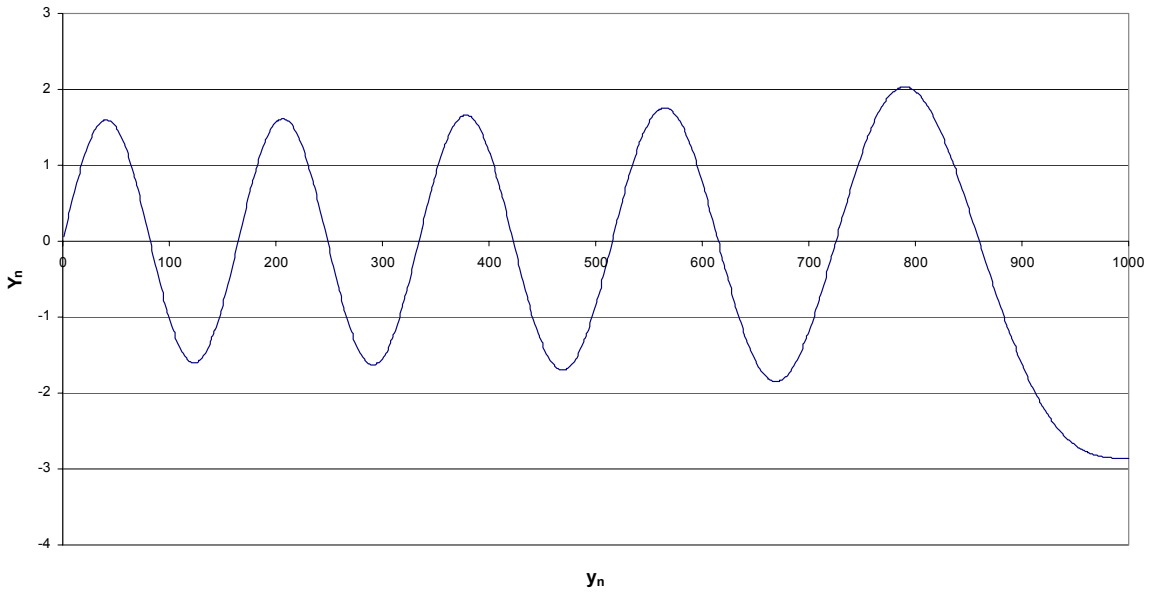

Figure 3-7: Plot of Tenth Eigenvector

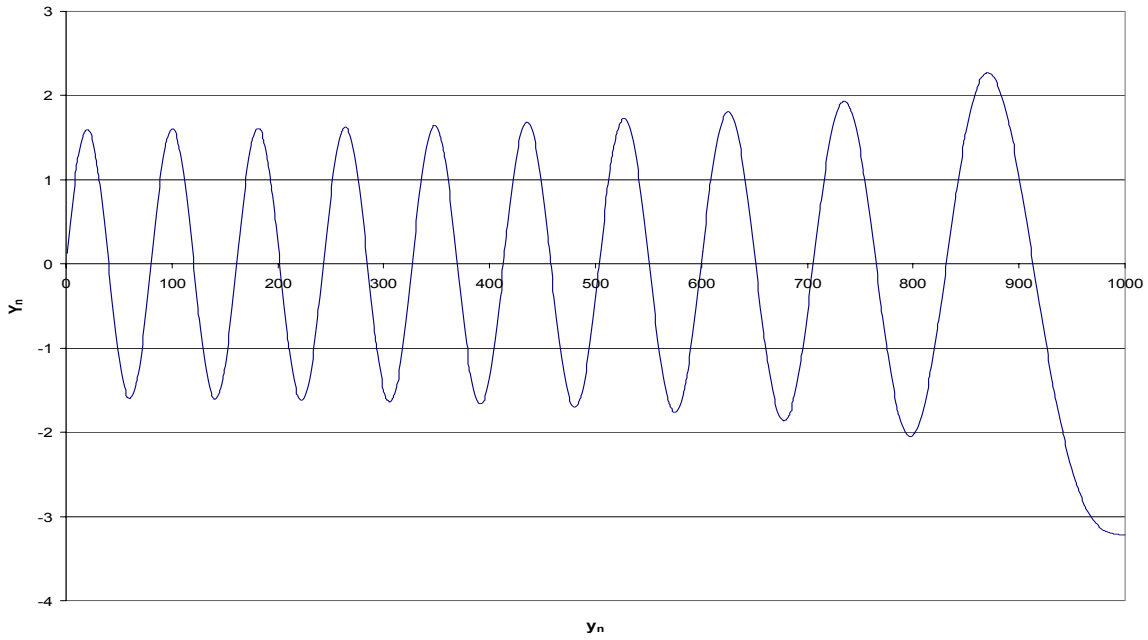

Figure 3-8: Plot of Twentieth Eigenvector

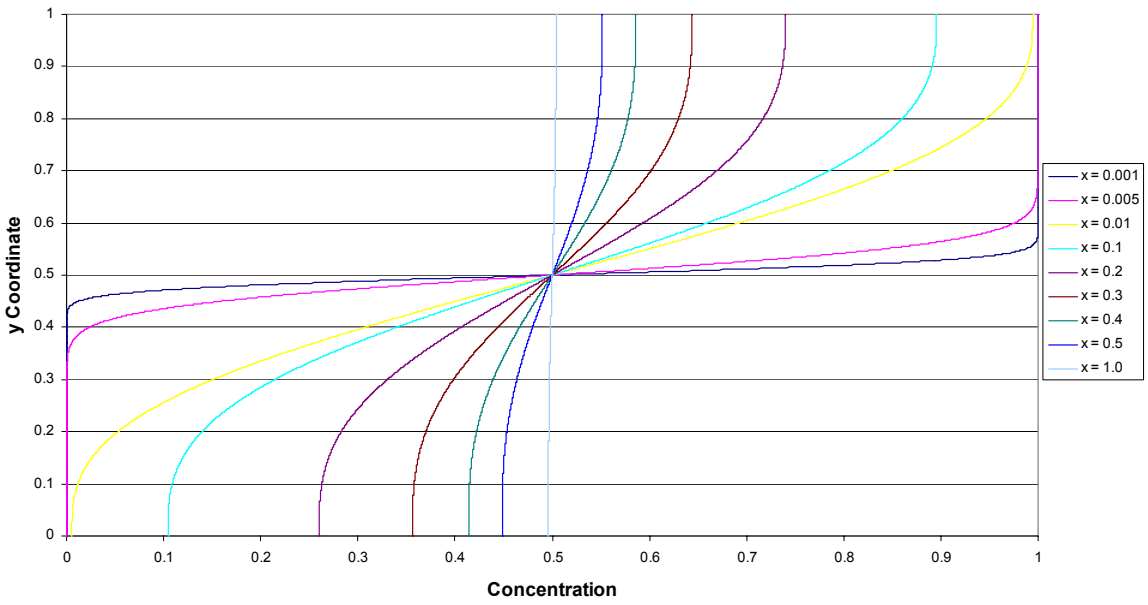

Figure 3-9: Model 2 Dimensionless Concentration as a Function of Non-Dimensional Position

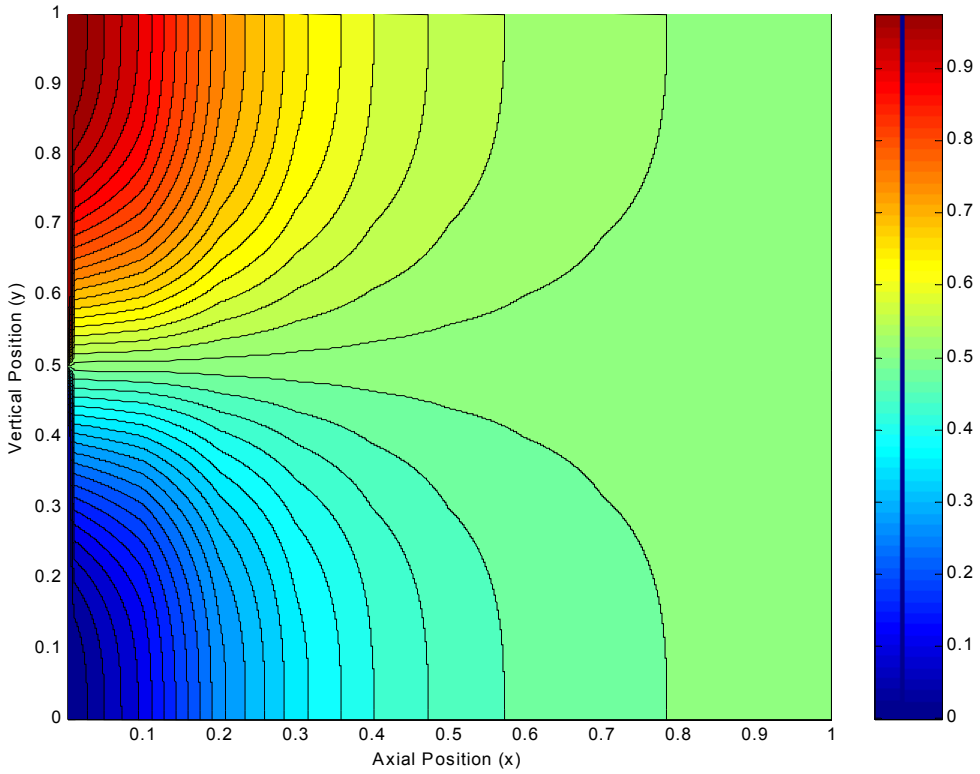

Figure 3-10: Contour Plot of Model 2Concentration as a Function of Non-Dimensional Position

the end of the micro-channel. Therefore with the proper selection of parameters such as pressure differential and channel height it can be possible to make a wave-guide of any desired length. That is assuming this model is accurate.

Chapter 4: Conclusion and Future Work

In modeling the diffusion within a micro channel flow problem two models were created. The first model was for the quiescent diffusion in a one-dimensional channel as a function of position and time. The second models the diffusion as two-dimensional flow within a channel with an assumed velocity profile. The diffusion in this model is a function of the velocity profile and the position within the micro channel. The velocity profile was taken to be that of plane Poiseuille flow for the upper half channel, with this profile the diffusion becomes only a function of position.

The driving force behind this research was the determining the length a micro channel could be before the diffusion of monomers from two different concentration solutions made the concentration drop to fifty percent. Using each of the models a length was determined. From these models, it can be seen that in order to have the longest wave-guide possible the fluid must flow through the micro channel with an imposed velocity; otherwise, the concentration within a stagnant flow drops below fifty percent halfway through the channel.

In solving the partial differential equations governing both of the models, the techniques of separation of variables and Fourier series were employed. In the first model, the equation was of a standard form that could be found in a mathematical textbook. The second model was not as easy; it required the solution of its eigenfunction problem through numerical techniques. Because the eigenfunction equation was so stiff many different techniques were tried until finally finding that the method of Finite Elements worked. The computer programs Mathematica and MatLab were used to perform the numerical computations involved in solving of the equation.

The next step for this analysis is to create a more accurate model. This means making fewer assumptions. This more accurate model would be fully three-dimensional and would not assume a velocity profile. Instead, the Navier-Stokes equations for incompressible flow would be solved, yielding the velocity within the micro-channel. This could then be used in the concentration equation yielding a more accurate result. In this case the use of a three dimensional element would need to be used in the Finite

Element model. Another thing still to be done is to compare the results obtained numerically with those obtained experimentally at NASA Marshall. If further refinements are found to be necessary then the flow will need to be modeled as an unsteady or transient flow.

References

1.) Bejan, Adrian, Convection Heat Transfer, John Wiley & Sons, New York, 1995

2.) Boyce, William E. and DiPrima, Richard C., Elementary Differential Equations and Boundary Value Problems, John Wiley & Sons, New York, 1965

3.) Cess, R. D., Shaffer, E. C. "Heat Transfer to Laminar Flow Between Parallel Plates with a Prescribed Wall Heat Flux," *Applied Science Research*, Section A, Vol. 8, 1959

4.) Haberman, Richard, Elementary Applied Partial Differential Equations, 3rd ed. Prentice Hall, NJ, 1998

5.) Panton, Ronald L., Incompressible Flow, 2nd ed. John Wiley & Sons, New York, 1996

6.) Rosenhead, L., Laminar Boundary Layers, Oxford at the Clarendon Press, Oxford, 1963.

7.) Sparrow, E. M., Novotny, J. L., Lin, S. H., "Laminar Flow of a Heat-Generating Fluid in a Parallel-Plate Channel," *American Institute of Chemical Engineering Journal* Vol. 9, No.6 November, 1963, 797-804

8.) Strang, Gilbert, Fix, George J., An Analysis of the Finite Element Method, Prentice-Hall, Inc, Englewood Cliffs, NJ, 1973

9.) Wolfram, Stephen, The Mathematica Book, 4th ed. Wolfram Media, Champaign, IL, 1999

Appendix

For n, m = 1……N-1

m = n-1,

$$M_{n,(n-1)} = \int_{(n-1)w}^{nw} \left(1-y^2\right)\left(1-\frac{1}{w}(y-nw)\right)\left(1+\frac{1}{w}(y-nw)\right)dy \quad (3\text{-}12)$$

m = n+1,

$$M_{n,(n+1)} = \int_{nw}^{(n+1)w} \left(1-y^2\right)\left(1-\frac{1}{w}(y-nw)\right)\left(1+\frac{1}{w}(y-nw)\right)dy \quad (3\text{-}13)$$

m = n

$$M_{n,n} = \int_{(n-1)w}^{nw} \left(1-y^2\right)\left(1+\frac{1}{w}(y-nw)\right)^2 dy + \int_{nw}^{(n+1)w} -\left(1-y^2\right)\left(1-\frac{1}{w}(y-nw)\right)^2 dy \quad (3\text{-}14)$$

For m = n = N

$$M_{N,N} = \int_{(N-1)w}^{Nw} \left(1-y^2\right)\left(1+\frac{1}{w}(y-Nw)\right)^2 dy \quad (3\text{-}15)$$

If |m-n| > 1

$M_{n,m} = 0$

$$M_{n,m} = \begin{vmatrix} 0.0659 & 0.0163 & 0 & 0 & 0 & 0 & 0 & 0 & 0 & 0 \\ 0.0163 & 0.0639 & 0.0156 & 0 & 0 & 0 & 0 & 0 & 0 & 0 \\ 0 & 0.0156 & 0.0606 & 0.0146 & 0 & 0 & 0 & 0 & 0 & 0 \\ 0 & 0 & 0.0146 & 0.0559 & 0.0133 & 0 & 0 & 0 & 0 & 0 \\ 0 & 0 & 0 & 0.0133 & 0.0499 & 0.0116 & 0 & 0 & 0 & 0 \\ 0 & 0 & 0 & 0 & 0.0116 & 0.0426 & 0.0096 & 0 & 0 & 0 \\ 0 & 0 & 0 & 0 & 0 & 0.0096 & 0.0339 & 0.0073 & 0 & 0 \\ 0 & 0 & 0 & 0 & 0 & 0 & 0.0073 & 0.0239 & 0.0046 & 0 \\ 0 & 0 & 0 & 0 & 0 & 0 & 0 & 0.0046 & 0.0126 & 0 \\ 0 & 0 & 0 & 0 & 0 & 0 & 0 & 0 & 0 & 0.0016 \end{vmatrix}$$

Equation A-1: Method for Producing Mass Matrix with Example of Ten Node Matrix

For n, m = 1……N-1

m = n-1,

$S_{n,(n-1)} = -N$

m = n+1,

$S_{n,(n+1)} = -N$

m = n

$S_{n,n} = 2*N$

For m = n = N

$S_{N,N} = N$

If |m-n| > 1

$S_{n,m} = 0$

$$S_{n,m} = \begin{vmatrix} 20 & -10 & 0 & 0 & 0 & 0 & 0 & 0 & 0 & 0 \\ -10 & 20 & -10 & 0 & 0 & 0 & 0 & 0 & 0 & 0 \\ 0 & -10 & 20 & -10 & 0 & 0 & 0 & 0 & 0 & 0 \\ 0 & 0 & -10 & 20 & -10 & 0 & 0 & 0 & 0 & 0 \\ 0 & 0 & 0 & -10 & 20 & -10 & 0 & 0 & 0 & 0 \\ 0 & 0 & 0 & 0 & -10 & 20 & -10 & 0 & 0 & 0 \\ 0 & 0 & 0 & 0 & 0 & -10 & 20 & -10 & 0 & 0 \\ 0 & 0 & 0 & 0 & 0 & 0 & -10 & 20 & -10 & 0 \\ 0 & 0 & 0 & 0 & 0 & 0 & 0 & -10 & 20 & -10 \\ 0 & 0 & 0 & 0 & 0 & 0 & 0 & 0 & -10 & 10 \end{vmatrix}$$

Equation A-2: Method for Producing Stiffness Matrix with Example of Ten Node Matrix

```
nodes=1000;
k=nodes;
n=1; While[n<nodes+1,m=0;While[m<nodes+1,M[n,m}=0;m++];n++];
w=1/k;
n=m=1;
While[n<nodes,m=0;
        While[m<nodes,
                If[m==n,
```

$$M[n,m]=\int_{(n-1)w}^{nw}(1-y^2)\left(1+\frac{1}{w}(y-nw)\right)^2dy+\int_{nw}^{(n+1)w}(1-y^2)\left(1-\frac{1}{w}(y-nw)\right)^2dy\ ];$$

```
                If[m==n+1,
```

$$M[n,m]=\int_{nw}^{mw}(1-y^2)\left(1+\frac{1}{w}(y-nw)\right)\left(1-\frac{1}{w}(y-nw)\right)dy\ ];$$

```
                If[m==n-1,
```

$$M[n,m]=\int_{mw}^{nw}(1-y^2)\left(1+\frac{1}{w}(y-nw)\right)\left(1-\frac{1}{w}(y-nw)\right)dy\ ];$$

```
                m++];n++];
```

$$M[k,k]=\int_{(k-1)w}^{kw}(1-y^2)\left(1+\frac{1}{w}(y-kw)\right)^2dy$$

```
Mk=Array[M,{nodes,nodes},1];
Mkn=Matrixform[Mk];
Export[“Mkn.dat”,N[Mkn],”Table”];
n=1; While[n<nodes+1,m=0;While[m<nodes+1,S[n,m}=0;m++];n++];
n=m=1;
While[n<nodes+1,m1;
        While[m<nodes+1,If[m==n,S[n,m]=k*2];
                If[m==n+1,S[n,m]=k*-1];If[m=n-1,S[n,m]=k*-1];m++];n++];
S[k,k]=k*1;
Sk=Array[S,{nodes,nodes},1];
Skn=MatrixForm[Sk];
Export[“Skn.dat”,N[Skn],”Table”];
```

Figure A-1: Mathematica Input Code for Creation of Mass and Stiffness Matrices

```
load Skn.dat
load Mkn.dat
b=eig(Skn,Mkn)
save b.out b -ASCII
[V,D]=eig(Skn,Mkn)
```

Figure A-2: MatLab Input Code for Solving Matrix Equation for Eigenvalues and Eigenvectors.

```
Import[“C:\\My Documents\\Rr. Antar\\FEA Solution\\try3\\1000
nodes\\V1.out”,”Table”]
Ev=Interpolation[%]
```

$$u = \int_0^1 Ev[y*100]*(1-y^2)dy$$

```
N[u]
```

Figure A-3: Mathematica input Code for Finding A_n

```
c=zeros(1000,10);
n=zeros(1000,20);
j=1;
while j<=10
        x=j/10;
        i=1;
        while i<=20
                n(:,i)=an(i)*V(:,i)*exp(-b(i)*x)
                i=i+1;
        end
        c(:,j)=sum(n')';
        j=j+1;
end
```

Figure A-4: MatLab Input Code for Finding Concentration within the Micro-Channel

Vita

Michael Kirsch was born in Bethpage, New York on August 8, 1978. He grew up in Bellmore, NY where he attended Saw Mill Elementary School, Grand Avenue Junior High School, and W. C. Mepham High School, where he graduated in June of 1996 with a Regents Diploma with Honors. In January of 1996 he earned the rank of Eagle Scout from the Boy Scouts of America. He continued his education at Polytechnic University's Long Island Campus, in Farmingdale, NY. He earned a Bachelor of Science in Aerospace Engineering in June 2000. In December 2000 he earned a second Bachelor's degree in Mechanical Engineering. His interest in spacecraft design led him to pursue a Master of Science Degree in Aerospace Engineering at the University of Tennessee Space Institute.

Mike plans to continue his education and pursue a PhD at the Joint Institute for the Advancement of Flight Sciences, a joint program between NASA Langley and George Washington University in Hampton, VA.